Journal of The Electrochemical Society, **158** (5) A498-A503 (2011)
0013-4651/2011/158(5)/A498/6/$28.00 © The Electrochemical Society

Passivating Ability of Surface Film Derived from Vinylene Carbonate on Tin Negative Electrode

Sangjin Park, Ji Heon Ryu, and Seung M. Oh[*,z]

Department of Chemical and Biological Engineering, WCU Program of C2E2, College of Engineering, Seoul National University, Seoul 151-744, Republic of Korea

The passivating ability of surface film derived from vinylene carbonate (VC) is addressed on tin (Sn) negative electrode after a comparative study on the thickness, film growth pattern, chemical composition, and mechanical flexibility of the surface films generated from VC-free and VC-added electrolytes. The surface film derived from the former electrolyte is enriched by inorganic fluorinated and carbonate species, and shows a poor passivating ability to cause a continued electrolyte decomposition, film growth and eventual electrode failure. In contrast, organic carbon-oxygen species are dominant in the film derived from the VC-added electrolyte. Even if this film is thinner than the other, it passivates the Sn electrode surface more effectively. As a result, the film growth and electrode polarization are less significant. The superior passivating ability of organic-rich surface film has been ascribed to a uniform coverage and higher mechanical flexibility.
 [DOI: 10.1149/1.3561424]

Manuscript submitted October 18, 2010; revised manuscript received February 2, 2011. Published March 18, 2011.

The Li-alloying materials (Si and Sn) have been developed as an alternative to the present graphitic carbons for lithium-ion batteries (LIBs).[1–4] The practical use of these high-capacity negative electrodes is, however, still limited due to their poor cycling behavior, which may be caused by: (i) cracking/crumbling of the active material (Si and Sn), (ii) electrical contact loss by a massive volume change during alloying/de-alloying, and (iii) continuous electrolyte decomposition and surface film formation, named solid electrolyte interphase (SEI).[5]

The electrolyte decomposition and concomitant film deposition are inevitable in the present LIBs since they operate far beyond the thermodynamic stability window of the common electrolytes. The successful commercialization of LIBs has, however, been possible since this surface film passivates the electrode surface, once it forms, to prevent additional electrolyte decomposition. In order for surface film to accomplish its own passivating role, the SEI layer should thus be compact and perfectly cover the electrode surface to prevent additional electrolyte decomposition. In addition, SEI layer should be thin to allow a fast Li^+ ion movement. The mechanical flexibility of surface film seems to be another important requirement particularly for the Li-alloying materials. Namely, inflexible surface film cannot effectively passivate the electrode surface since it is easily broken or deformed by the massive volume change evolved with the Li-alloying materials, leading to an exposure of electrode surface to electrolyte solution.

The SEI formation mechanism on the Li-alloying materials is somewhat different to that on the carbonaceous negative electrodes. On graphite surface, SEI layer forms within a few initial cycles, whereas the film formation is continued on the Li-alloying materials since new electrode surface is generated as a result of continued cracking/crumbling. The film growth patterns are much more complicated on the Li-alloying materials. As a result, the SEI study on the Li-alloying materials is still limited, while those on graphite electrodes are numerous.[6,7]

The prime concern in this work is to assess the passivating ability of surface film derived from vinylene carbonate (VC), which is one of the common SEI formers.[8,9] To this end, a comparative study is made on the surface films derived from the VC-added and VC-free electrolyte, from which the passivating ability of VC-derived surface film is addressed. In details, the passivating ability is assessed by measuring the reduction current associated with the electrolyte decomposition on an exposed Sn electrode surface. To estimate the mechanical flexibility, a bending experiment is devised, in which the Sn electrode is bent after surface film deposition. An expectation here is that, if the surface film is not mechanically flexibility, it is deformed by bending to generate new Sn surface, onto which electrolyte decomposition is induced. To account for the difference in passivating ability and mechanical flexibility for two surface films, the chemical compositions are analyzed by using depth-profiling x-ray photoelectron spectroscopy (XPS) and Fourier-transform infrared spectroscopy (FT-IR), whereas the film growth pattern and thickness are estimated from the cross-sectional scanning electron microscope (SEM) images of the cycled electrodes.

Experimental

The Sn film was electro-deposited on a piece of copper foil in a plating bath composed of 0.14 *M* tin (II) sulfate ($SnSO_4$), 0.34 *M* potassium sulfate (K_2SO_4), and 0.42 *M* sodium *d*-gluconate ($C_6H_{11}O_7Na$). The electro-deposition was performed at a current density of 5 mA cm^{-2} for 8 min at room temperature.

Electrochemical performances of the Sn film negative electrodes were examined using a coin-type cell (2032-type), which was fabricated by inserting a polypropylene separator (20 μm) between the Sn film electrode and lithium foil (Cyprus Co.). The used electrolyte was 1.0 *M* lithium hexafluorophosphate ($LiPF_6$) dissolved in ethylene carbonate (EC) and dimethyl carbonate (DMC) (1:1, volume ratio), in which 5 wt. % of VC was added. Galvanostatic charge/discharge cycling was made at a current density of 400 mA g^{-1} in the voltage range of 0.01–1.2 V (vs. Li/Li^+).

For a post mortem field-emission SEM (Model JSM-6700F, JEOL), XPS and FT-IR analyses, the cells were dismantled in a glove box and the electrodes were washed with dimethyl carbonate. A hermetic vessel was used to transfer the samples from the glove box to the instrument chamber. The XPS data were collected in an ultra-high vacuum multipurpose surface analysis system (Sigma probe, Thermo, UK) that operates at a base pressure of $<10^{-10}$ mbar. The photoelectrons were excited by Al Kα (1486.6 eV) radiation at a constant power of 150 W (15 kV and 10 mA); the x-ray spot size was 400 μm. During data acquisition, a constant-analyzer-energy mode was used at a pass energy of 30 eV and a step of 0.1 eV. The depth-profiling XPS measurement was made by a continued Ar^+ ion sputter etching and the chemical composition was estimated by using the atomic sensitivity factor.[10,11] For the cross-sectional images, the electrode samples were crosscut by using an Ar^+ ion beam polisher (SM-09010, JEOL) at a constant power of 0.5 W (5 kV and 0.1 mA) under vacuum ($<2.0 \times 10^{-4}$ Pa). The infrared spectra were obtained using the attenuated total reflection (ATR) mode (Nicolet 5700 FT-IR spectrometer). The cycled electrodes were mounted on an internal reflection crystal (Ge) facing the surface layer toward the crystal. For the bending experiment, a pouch-type cell was fabricated with the Sn film electrode (3 × 3 cm), polypropylene separator and lithium foil. In this report, the lithiation (alloying) is expressed as discharging, whereas the de-lithiation (de-alloying) charging on the basis of the standard lithium-ion cell configuration.

* Electrochemical Society Active Member.
z E-mail: seungoh@snu.ac.kr

Results and Discussion

Figure 1 compares the lithiation and de-lithiation voltage profiles obtained with the Li/Sn cells in the VC-free and VC-added electrolyte.

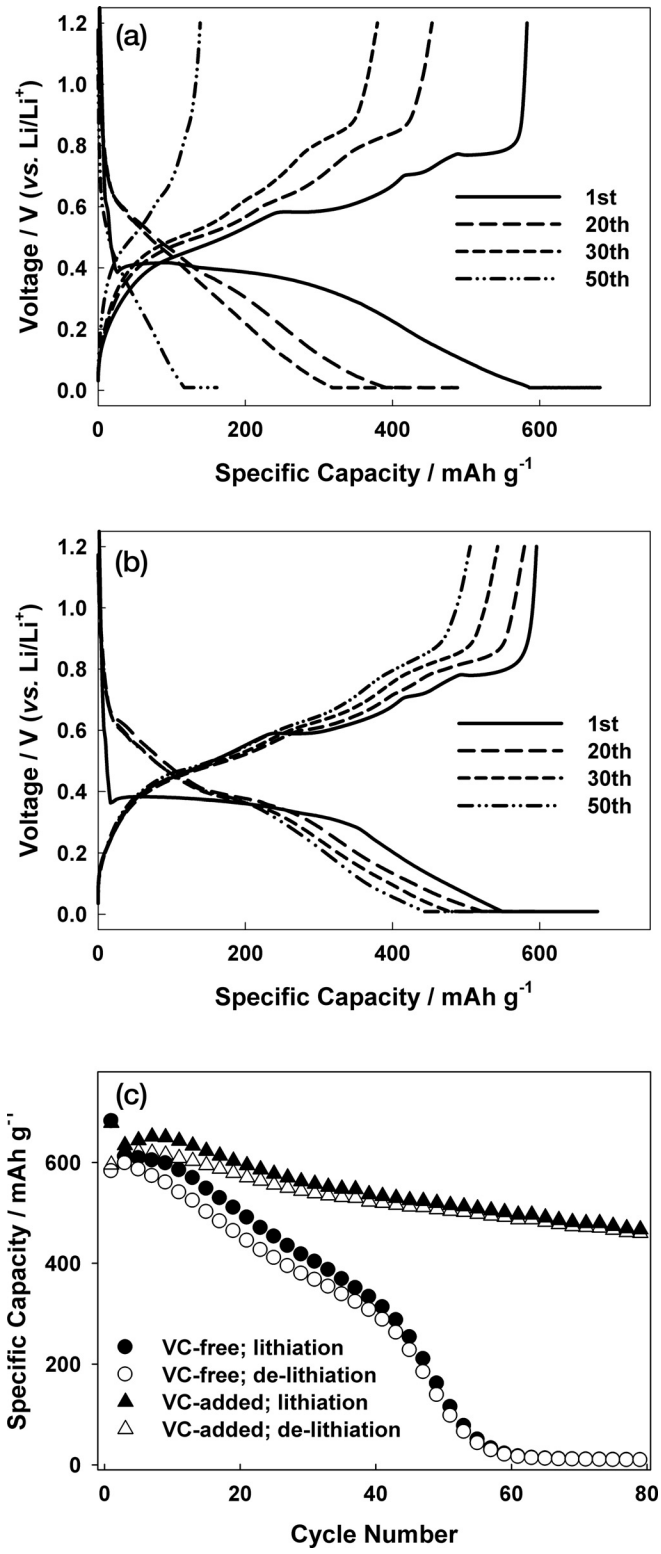

Figure 1. Galvanostatic discharge (lithiation, downward) and charge (de-lithiation, upward) voltage profiles obtained with Li/Sn film cell in: (a); VC-free electrolyte and (b); VC-added electrolyte. The cycle performance is compared in (c). Current density = 400 mA g^{-1}. Voltage cut-off = 0.01–1.2 V (vs. Li/Li^+).

In the first cycle, the Sn negative electrode shows a comparable charge-discharge behavior in two electrolytes with a lithiation capacity of ca. 680 mA h g^{-1} and coulombic efficiency of >85%. From the second cycle, however, the Sn electrode delivers a different cycle performance in two electrolytes. A severe capacity fading is observed in the VC-free electrolyte, whereas a much better cycle performance in the VC-added electrolyte with a de-lithiation capacity amounting to >85% of the initial value even after 50 cycles (Fig. 1c). The poor cycle performance in the VC-free electrolyte seems to be deeply associated with the electrode polarization that steadily increases with cycling (Fig. 1a). Also noted in Fig. 1c is that the Sn film electrode shows an irreversible capacity in every cycle, implying that the electrolyte decomposition and Li^+ trapping inside the "dead" Sn grains are continued with cycling. The detailed discussion on this will be advanced in the later section.

The surface and cross-sectional images of the pristine Sn film electrode are displayed in Figs. 2a and 2b, respectively. The Sn grains of 1–2 μm are deposited on the Cu foil (Fig. 2a) and the Sn layer thickness is ca. 1 μm (Fig. 2b). The cross-sectional images of the cycled electrodes are also presented in Figs. 2c–2h. The following points should be noted. First, both the surface film and Sn layer

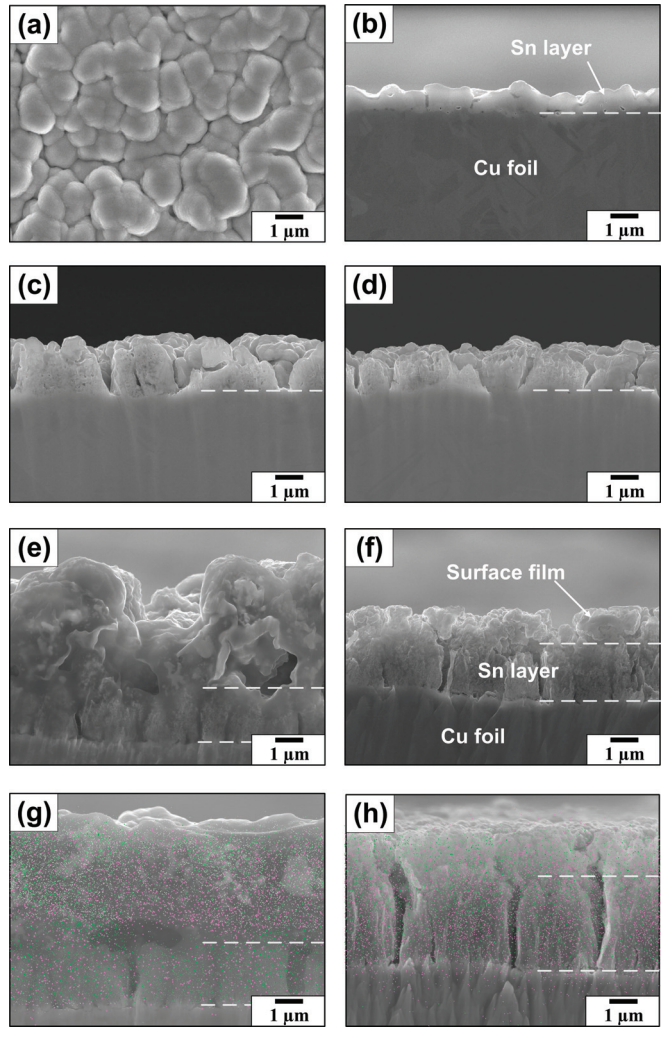

Figure 2. (Color online) FE-SEM images of the Sn film electrode before cycling: (a); top view and (b) side view. The cross-sectional images of Sn film electrodes cycled in the VC-free (left panel) and VC-added electrolyte (right panel): (c)/(d); after 5 cycles, (e)/(f); after 10 cycles, and (g)/(h); after 20 cycles. The EDS mappings are presented in (g)/(h). The pink and green points correspond to C and Sn element, respectively. The images in (c)–(h) were obtained after a full de-lithiation.

expands to the normal direction with cycling, implying that the electrolyte decomposition and electrode swelling are continued with cycling. Second, the growth of surface film is more prominent in the VC-free electrolyte (left panel). Third, the population of Sn (green points) is not confined within the initial Sn layer, rather extended to the surface film layer as seen on the EDS mappings (Figs. 2g and 2h). This illustrates that the Sn grains are cracked/crumbled with cycling and some of them move from the initial Sn layer to the surface film layer to be embedded into the surface film. A high population of carbon (pink points) is also noticed in the Sn layer, reflecting that the carbon-containing film forms not only in the surface film layer but also within the Sn layer. From these, the following scenario is assumed for the film formation. The Sn grains expand with alloying but do not contract to the initial dimension upon de-alloying, leading to an electrode layer expansion with cycling.[6,12,13] During this volume change, the Sn grains are cracked/crumbled due to mechanical stress, and some of the fine Sn grains are detached from the Sn layer. Then, additional electrolyte decomposition and film deposition take place on the fresh Sn surfaces that are exposed inside the cracks.[1,8,9,13,14] The high population of carbon in the Sn layer explains this feature. Film deposition is also possible on the detached Sn grains if they are electrically connected to the Sn layer and Cu foil. Due to the continued film growth, which is electrically insulating, the detached Sn grains are even more electrically isolated from the Sn layer to be inactive ("dead") as the negative electrode. The irreversible capacity appearing in every cycle (Fig. 1c) can thus be ascribed to the Li^+ trapping inside these dead Sn grains as well as the electrolyte decomposition on the newly exposed Sn surface. The capacity fading shown in Fig. 1 can also be accounted for by the continued film growth and dead Sn formation. That is, the thicker surface film generated from the VC-free electrolyte leads to the larger electrode polarization due to impeded Li^+ ion diffusion. Due to this polarization, the lithiation voltage reaches the lower cut-off earlier during the galvanostatic cycling, leading to a decrease in the lithiation and de-lithiation capacity. The substantial capacity fading in the VC-free electrolyte can also be explained by the generation of dead Sn. As seen in Figs. 2g and 2h, the initial Sn layer becomes thinner in the VC-free electrolyte, suggesting that a larger amount of Sn grains are detached, such that the formation of dead Sn is more probable in this electrolyte.

As shown in Fig. 2, the film growth rate differs in two electrolytes. Given that film does not grows if surface film effectively passivates electrode surface, it is likely that the passivating ability is better for the surface film generated from the VC-added electrolyte. To ensure the difference in passivating ability, cyclic voltammograms were obtained after the film formation in two electrolytes. This experiment was inspired by the previous reports that the catalytic reductive decomposition of electrolytes takes place near 1.5 V (vs. Li/Li^+) on a fresh Sn surface.[15–17] In order for this current to be detected, the lithiated Sn (Li_xSn) should be converted to metallic Sn, and furthermore the as-generated Sn is exposed to the electrolyte solution since this reduction current evolves only on the Sn surface exposed to electrolyte solution, not on either the Li-Sn alloy surface or the Sn surface covered by passivation layer. Two features should be noted in the cyclic voltammograms shown in Fig. 3. First, the oxidation current appears in both electrolytes during the potential sweep from 1.2 to 2.0 V, which is associated with the de-alloying reaction of the Li_xSn phases.[15–17] The larger oxidation current with the thicker surface films illustrates that a larger amount of Li_xSn phases still remains at the last de-lithiation period of the film generation step due to slower Li^+ diffusion through the thicker films. Second, the reduction current appears at 1.5 V when the electrode potential moves from 2.0 to 0.8 V in the VC-free electrolyte (Fig. 3a). This illustrates that the metallic Sn is restored upon de-alloying up to 2.0 V, on which the reductive electrolyte decomposition takes place due to poor passivating ability of the surface film. In contrast, the reduction current is not detected with the VC-derived surface films, even with the thinnest one deposited by five charge/discharge cycles (Fig. 3b). Clearly, the VC-derived surface film is more passivating even if it is thinner than that forms in the VC-free electrolyte.

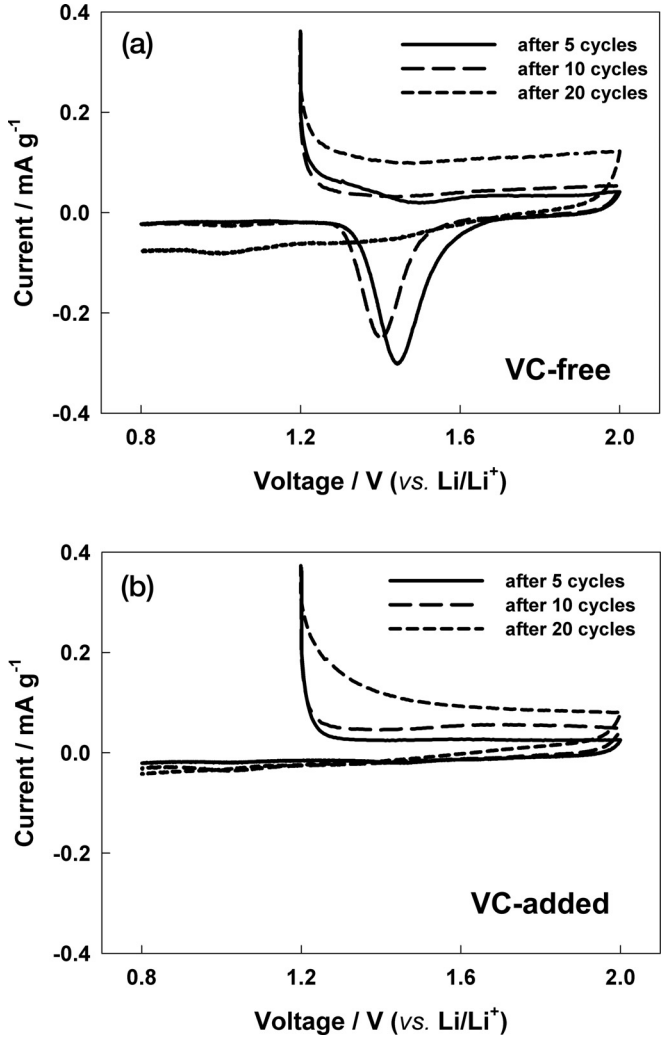

Figure 3. Cyclic voltammograms obtained after the film deposition with the predetermined number of cycling. After the surface film deposition, the electrode potential was moved from 1.2 to 2.0 V (vs. Li/Li^+) to convert the lithiated Sn (Li_xSn) to metallic Sn and then from 2.0 to 0.8 V to detect the catalytic reduction current.

To gain an insight into the factors affecting the passivating ability, the chemical composition and thickness of two surface films are analyzed by using XPS. The C 1s, O 1s and F 1s photoelectron spectra are represented in Fig. 4. The C 1s spectra were fitted with four peaks according to the reported binding energies; $ROCO_2Li$ (CO_3-like) at 290 eV, O=C-O at 288 eV, C-O at 286.5 eV, and CH_2 at 285 eV.[12,18–21] All these photoelectrons must be emitted from the surface films since the Sn film electrode does not contain any carbon species such as polymeric binder and conductive carbon. As seen in the C 1s spectra, the population of carbon-oxygen species is higher in the film derived from the VC-added electrolyte. The enriched population of carbon-oxygen species in this film is further confirmed from the O 1s spectra. In Fig. 4b, the O 1s spectra are fitted with three broad peaks centered at 534.4 eV (poly vinylene carbonate), 533.5 eV (oxygen bound to carbon with a single bond in organic carbonates) and 532 eV (Li_2CO_3 and oxygen atoms doubly bound to carbon atoms in organic carbonates).[10,18,22] The high population of carbon-oxygen species in the VC-derived film is contrasted by the enriched deposition of inorganic fluorinated species (mainly LiF) that must be derived from the salt ($LiPF_6$) in the VC-free electrolyte (Fig. 4c). The stronger F 1s peaks are observed in this surface film, which corresponds to LiF (685.2 eV) and Li_xPF_y (687–688 eV).[10,18,21,23,24]

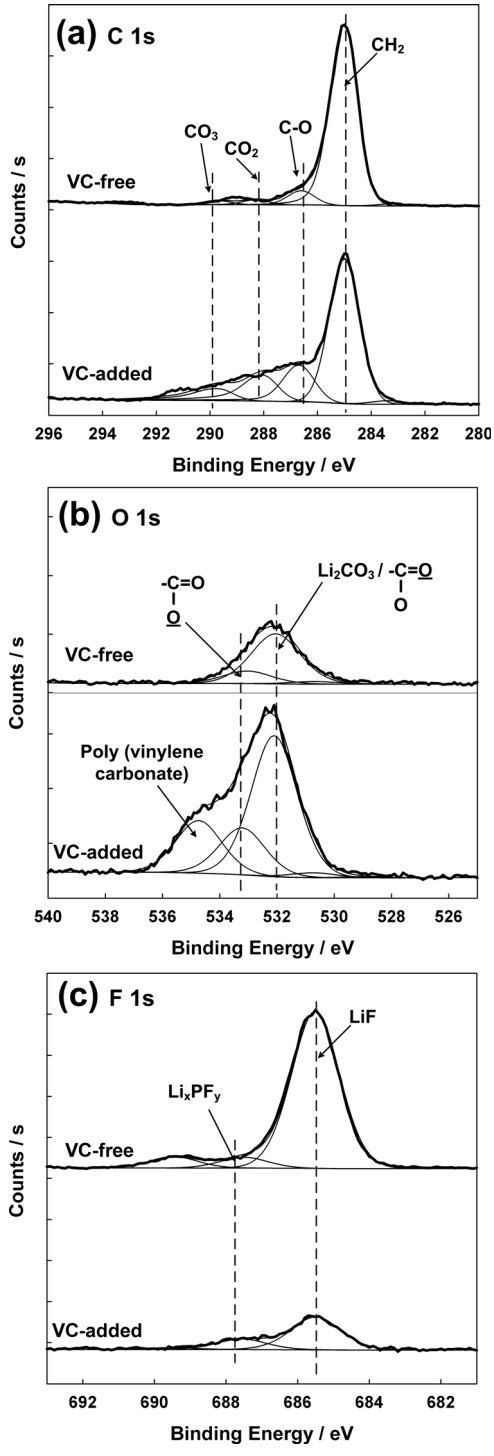

Figure 4. XPS spectra obtained with the surface films derived from the VC-free and VC-added electrolyte. The measurement was made after the first lithiation. Note that the spectra were obtained before the depth-profiling measurement, such that the photoelectrons are emitted from the topmost surface layer.

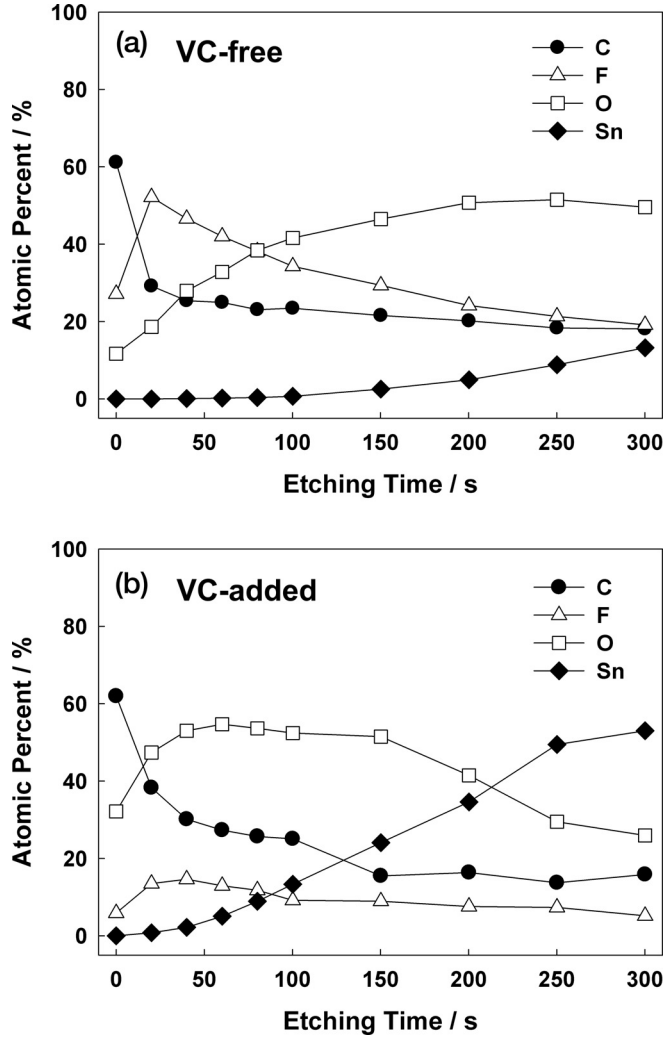

Figure 5. The variation of chemical composition as a function of film depth. The results were obtained by fitting the depth-profiling XPS data. The measurement was made after the first lithiation.

The two surface films differ in chemical composition not only at the topmost region (Fig. 4) but also in the deeper region as shown in the depth-profiling XPS data (Fig. 5), in which the atomic concentration of four elements is plotted as a function of etching time. The higher population of fluorinated species is noted even in the deeper region of the film derived from the VC-free electrolyte (Fig. 5a), whereas the carbon-oxygen species are dominant over the fluorinated ones in the VC-derived film (Fig. 5b). The carbon-oxygen species must come from either the carbonate solvent (EC and DMC in this work) or VC. Of the two, however, VC seems to be the more probable source since this unsaturated carbonate is more vulnerable to reductive decomposition than the saturated counterparts.[25–29] Another important observation in Fig. 5 is that the VC-derived surface film is thinner than the other as evidenced by the earlier exposure of Sn surface in the depth-profiling experiment. Namely, the atomic percent of Sn is less than 20% even if the film in Fig. 5a is sputter etched for 300 s, but this value reaches 60% after the same period of etching on the VC-derived film. The earlier exposure of Sn in the latter illustrates the presence of a thinner surface film to be removed on the Sn electrode surface.

Figure 6 displays the FT-IR spectra obtained with two surface films, in which a deposition of lithium carbonate (Li_2CO_3) and lithium alkyl carbonate ($ROCO_2Li$) is observed. The peaks indexed by Δ [1493 and 1436 cm^{-1} ($\nu_{C\text{-}O,as}$), 1096 cm^{-1} ($\nu_{C\text{-}O,s}$), and 869 cm^{-1} (δ_{CO3})] can be assigned to the infrared absorptions by Li_2CO_3, whereas the peaks indicated by ↓ (1647 cm^{-1} ($\nu_{C=O,as}$) and 1317 cm^{-1} ($\nu_{C=O,s}$)) to those for lithium alkyl carbonate ($ROCO_2Li$).[30–32] The other vibrational absorptions for lithium alkyl carbonate at 1400 cm^{-1} ($\delta_{CH3,\ CH2}$) and 1074 cm^{-1} ($\nu_{C\text{-}O}$) cannot be located since they overlap with those for Li_2CO_3. Two major differences can be noticed in the IR spectra. First, the film derived from the VC-added electrolyte contains the decomposition products of VC, of which the absorption peaks are indicated by ↑ in Fig. 6. The peak at 1815 cm^{-1}

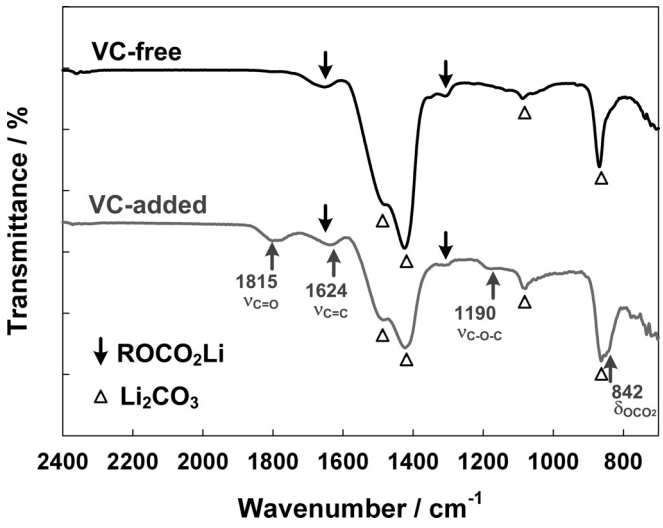

Figure 6. FT-IR spectra obtained with the surface films derived from VC-free and VC-added electrolyte. The measurement was made after the first lithiation.

can be assigned to the stretching vibration of C=O bonds in poly (vinylene carbonate) and that at 1624 cm^{-1} to the stretching of C=C bonds.[28] As the double-bond containing products to be derived from VC, lithium vinylene carbonate (C=$COCO_2Li$) and lithium vinylene alkoxide (C=COLi) have been proposed.[25,28] Second, the population of organic carbon-oxygen species is larger in the film derived from the VC-added electrolyte. That is, a comparison of two spectra reveals that the absorption peaks belonging to the organic C-O species (for instance, $ROCO_2Li$ and VC-derived ones) are larger in the film derived from the VC-added electrolyte at the expense of those for the inorganic species (Li_2CO_3).

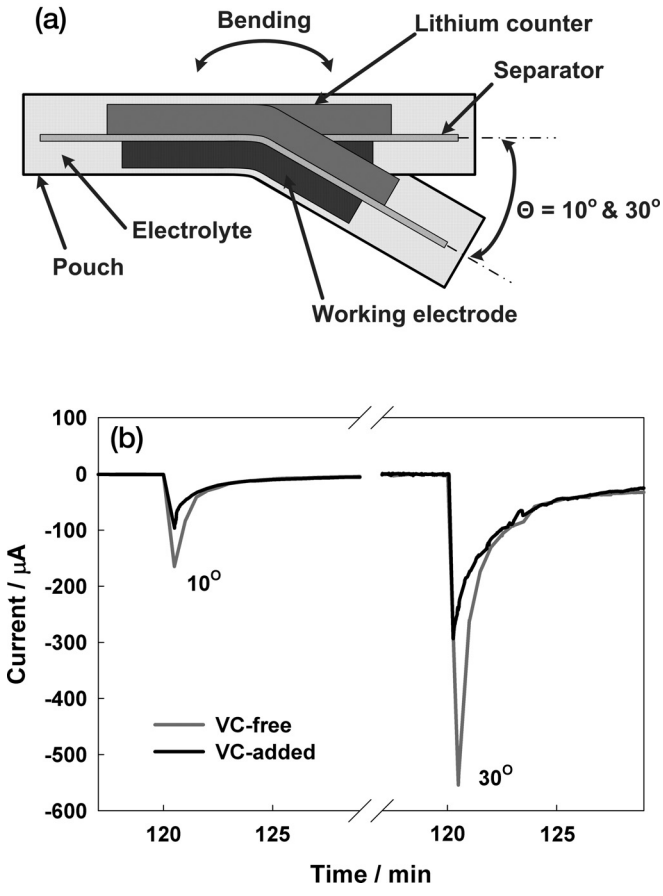

Figure 7. (a); Schematic illustration for the bending experiment and (b); the reduction current observed after the bending. To generate surface films, the potential of Sn film electrode was fixed at 0.01 V (vs. Li/Li^+) for 2 h. The pouch-type cells were then bent by 10 and 30° while the electrode potential being fixed at 0.01 V. The reduction current associated with electrolyte decomposition on lithiated Sn (Li_xSn) was traced.

By combining the XPS, FT-IR spectra and the film growth pattern shown in Fig. 2, the factors affecting the passivating ability of surface films may be delineated. An assumption can be made from the experimental observations that organic-rich surface films have a stronger passivating ability than inorganic-rich ones, probably due to a more uniform coverage and higher degree of compactness. An ensuring feature is that the surface film deposited from VC in the first cycle is organic-rich (Fig. 5). Even if this film is thinner, the film growth is less significant from the second cycle (Fig. 2). In contrast, the inorganic-rich film is less passivating to allow a continued film growth (Fig. 2). In order for any thin surface films to have a strong passivating ability, they must be uniformly covered with a high degree of compactness. To draw a conclusion that organic-rich films have a superior passivating ability to inorganic-rich ones, however, additional experimental data should be collected. Also the reasons why organic species are more passivating should be studied.

Figure 7 presents the schematic illustration for the bending experiment and the current evolution observed after the electrode bending. The reduction current relevant to the electrolyte decomposition on Li_xSn is larger when the electrode is bent by a larger angle in both electrolytes. This must be due to a higher degree of film deformation to lead an enlarged exposure of Li_xSn surface to the electrolyte. The reduction current is, however, smaller for the film generated from VC, suggesting that the VC-derived surface film is mechanically more flexible. This favorable mechanical property seems to be inherited by the high population of organic species rather than inorganic ones in the VC-derived film. Furthermore, the higher passivating ability of this film seems to be partly originated by the higher flexibility. With this flexible film, the exposure of electrode surface to electrolyte solution seems less likely since the film is not easily broken or deformed upon a massive volume change of the Sn component.

Conclusions

The physicochemical properties of surface films derived from the VC-free and VC-added electrolyte were examined, from which the role of VC as a surface-film former has been addressed. The following points are summarized.

1. The surface films steadily grow with cycling in both VC-free and VC-added electrolyte. However, a thicker film is deposited from the VC-free electrolyte. The Sn electrode shows a poorer cycle performance in this electrolyte with a larger electrode polarization, which is caused by a slower Li^+ diffusion through the thicker surface layer. The VC-derived surface film is, however, thinner and cycle performance is better in this electrolyte with a less significant polarization.
2. The Sn grains are crumbled with cycling and some of fine Sn grains move to the surface film layer. The generation of this "dead" Sn seems to be an important degradation mechanism prevailing in this Li-alloying negative electrode.
3. In the first lithiation, organic-rich surface film is deposited in the VC-added electrolyte. Even if this film is thin, it effectively passivates the Sn surface to suppress additional electrolyte decomposition. In the VC-free electrolyte, however, a surface film enriched by inorganic fluorinated and carbonates species is generated. This film shows a poorer passivating ability probably due to non-uniform coverage and poor mechanical flexibility.

Acknowledgments

This research was supported by WCU program through the National Research Foundation of Korea funded by the Ministry of

Education, Science and Technology (R31-10013). The authors also wish to acknowledge the Research Center for Energy Conversion and Storage for financial support.

Seoul National University assisted in meeting the publication costs of this article.

References

1. S. C. Chao, Y. C. Yen, Y. F. Song, Y. M. Chen, H. C. Wu, and N. L. Wu, *Electrochem. Commun.*, **12**, 234 (2010).
2. M. Winter and R. J. Brodd, *Chem. Rev.*, **104**, 4245 (2004).
3. R. A. Huggins, *J. Power Sources*, **81–82**, 13 (1999).
4. C. J. Wen and R. A. Huggins, *J. Electrochem. Soc.*, **128**, 1181 (1981).
5. M. Winter and J. G. O. Besenhard, *Electrochim. Acta*, **45**, 31 (1999).
6. J. O. Besenhard, J. Yang, and M. Winter, *J. Power Sources*, **68**, 87 (1997).
7. J. Yang, M. Winter, and J. O. Besenhard, *Solid State Ionics*, **90**, 281 (1996).
8. H. Mukaibo, T. Momma, Y. Shacham-Diamand, T. Osaka, and M. Kodaira, *Electrochem. Solid-State Lett.*, **10**, A70 (2007).
9. I. A. Courtney, W. R. McKinnon, and J. R. Dahn, *J. Electrochem. Soc.*, **146**, 59 (1999).
10. R. Dedryvere, S. Laruelle, S. Grugeon, L. Gireaud, J. M. Tarascon, and D. Gonbeau, *J. Electrochem. Soc.*, **152**, A689 (2005).
11. J. H. Scofield, *J. Electron Spectrosc. Relat. Phenom.*, **8**, 129 (1976).
12. K. K. D. Ehinon, S. Naille, R. Dedryvere, P. E. Lippens, J. C. Jumas, and D. Gonbeau, *Chem. Mater.*, **20**, 5388 (2008).
13. M. Wachtler, J. G. O. Besenhard, and M. Winter, *J. Power Sources*, **94**, 189 (2001).
14. S. Yang, P. Y. Zavalij, and M. S. Whittingham, *Electrochem. Commun.*, **5**, 587 (2003).
15. I. T. Lucas, E. Pollak, and R. Kostecki, *Electrochem. Commun.*, **11**, 2157 (2009).
16. J. Hassoun, P. Reale, and S. Panero, *J. Power Sources*, **174**, 321 (2007).
17. S. D. Beattie, T. Hatchard, A. Bonakdarpour, K. C. Hewitt, and J. R. Dahn, *J. Electrochem. Soc.*, **150**, A701 (2003).
18. L. El Clualtania, R. Dedryvere, J. B. Ledeuil, C. Siret, P. Biensan, J. Desbrieres, and D. Gonbeau, *J. Power Sources*, **189**, 72 (2009).
19. H. Bryngelsson, M. Stjerndahl, T. Gustafsson, and K. Edstr, *J. Power Sources*, **174**, 970 (2007).
20. R. Dedryvere, L. Gireaud, S. Grugeon, S. Laruelle, J. M. Tarascon, and D. Gonbeau, *J. Phys. Chem. B*, **109**, 15868 (2005).
21. A. M. Andersson, M. Herstedt, A. G. Bishop, and K. Edstrom, *Electrochim. Acta*, **47**, 1885 (2002).
22. Y.-C. Lu, A. N. Mansour, N. Yabuuchi, and Y. Shao-Horn, *Chem. Mater.*, **21**, 4408 (2009).
23. L. Daheron, R. Dedryvere, H. Martinez, M. Menetrier, C. Denage, C. Delmas, and D. Gonbeau, *Chem. Mater.*, **20**, 583 (2008).
24. M. Stjerndahl, H. Bryngelsson, T. Gustafsson, J. T. Vaughey, M. M. Thackeray, and K. Edstrom, *Electrochim. Acta*, **52**, 4947 (2007).
25. L. Chen, K. Wang, X. Xie, and J. Xie, *J. Power Sources*, **174**, 538 (2007).
26. S. S. Zhang, *J. Power Sources*, **162**, 1379 (2006).
27. L. B. Chen, K. Wang, X. H. Xie, and J. Y. Xie, *Electrochem. Solid-State Lett.*, **9**, A512 (2006).
28. H. Ota, Y. Sakata, A. Inoue, and S. Yamaguchi, *J. Electrochem. Soc.*, **151**, A1659 (2004).
29. D. Aurbach, K. Gamolsky, B. Markovsky, Y. Gofer, M. Schmidt, and U. Heider, *Electrochim. Acta*, **47**, 1423 (2002).
30. J.-T. Li, S.-R. Chen, X.-Y. Fan, L. Huang, and S.-G. Sun, *Langmuir*, **23**, 13174 (2007).
31. D. Aurbach, B. Markovsky, A. Shechter, Y. Ein-Eli, and H. Cohen, *J. Electrochem. Soc.*, **143**, 3809 (1996).
32. S. Oohira, M. Kakihana, Y. Fujii, T. Nagumo, and M. Okamoto, *J. Nucl. Mater.*, **133–134**, 201 (1985).